J Mater Sci (2010) 45:4912–4918
DOI 10.1007/s10853-010-4466-8

ICAM 2009

Phase transitions and piezoelectric properties of $SrBi_2Ta_2O_9$ by molecular dynamics simulations

R. Machado · M. Sepliarsky · M. G. Stachiotti

Received: 6 October 2009 / Accepted: 3 April 2010 / Published online: 22 April 2010

Abstract The phase transition sequence of $SrBi_2Ta_2O_9$ (SBT) and the local microscopic dynamics near the ferroelectric transition are investigated using a shell model with parameters fitted to first-principle calculations. We show that the complex interplay between polar and nonpolar instabilities leads to the presence of two phase transitions. In this way the existence of an intermediate orthorhombic paraelectric phase, characterized by the rotation of the TaO_6 octahedra, is demonstrated without using any explicit experimental data as input. The local polarization dynamics does not provide any indication of a relaxation process near the ferroelectric transition. Finally, dielectric and piezoelectric coefficients along crystallographic directions are investigated.

Introduction

$SrBi_2Ta_2O_9$ (SBT) is a ferroelectric material with many important technological applications due to its diverse physical properties which lead to its use in nonvolatile memories [1], and electromechanical applications at high temperatures [2]. In order to understand and optimize these applications, a detailed understanding of the material properties at the atomic level is essential, and computer modeling can play an important role here. However, the atomistic simulation of SBT and other Aurivillius compounds is a theoretical challenge, not only for the complexity of their crystal structures, which is highly anisotropic, but also for the delicate interplay between polar and nonpolar instabilities.

SBT belongs to the family of bismuth layered Aurivillius compounds having the formula $Bi_2O_2(A_{m-1}B_mO_{3m+1})$, where A = mono-,di-, or trivalent cations such as Na^+, Sr^{2+}, Ca^{2+}, Ba^{2+}, Pb^{2+}, or Bi^{3+}, B = Ti^{4+}, Ta^{5+}, Nb^{5+}, or W^{6+}, and m = 1–6 [3]. Many of these compounds are ferroelectric with high transition temperatures. Ferroelectricity in SBT was discovered by Smolenskii et al. [4]. For m = 2 or 4 (''even layer'' materials), it has now been well established that the ferroelectric phase adopts the orthorhombic space group $A21am$, which may be considered as derived from an archetypal tetragonal parent phase, space group $I4/mmm$. In SBT, for example, three main distortions from the paraelectric tetragonal structure lead to the ferroelectric phase: the ions displace along the orthorhombic a-axis (the [110] direction of the tetragonal structure), and TaO_6 octahedra rotate around the a and c axes [5]. The first factor is directly responsible for the macroscopic spontaneous polarization along the a direction, which mainly involves displacements of the Bi_2O_2 planes relative to the perovskite-like blocks [6]. Recent ab initio calculations combined with a structural and symmetry analysis demonstrated that a delicate interplay exists between these three structural instabilities, and the ferroelectric phase transition was explained by coupling the ferroelectric soft mode with another hard vibration associated with the octahedral tilting at the Brillouin zone boundary [7]. In this respect, the nature and sequence of phase transitions in SBT is much more complicated as compared to simple perovskites.

The nature of the ferroelectric–paraelectric phase transition in these materials has been uncertain until quite recently. In early studies using birefringence measurements [8], it was suggested that some phases of this type

R. Machado · M. Sepliarsky (✉) · M. G. Stachiotti
Instituto de Física Rosario, Universidad Nacional de Rosario,
27 de Febrero 210 Bis, 2000 Rosario, Argentina
e-mail: sepli@ifir-conicet.gov.ar

underwent a two-step transition from *A*21*am*, via an intermediate phase, to tetragonal *I*4/*mmm*. Observations made using electron diffraction at elevated temperature supported this hypothesis [9] but the exact nature of the transition remained unclear. Structural studies in polycrystalline SBT samples showed the existence of the intermediate phase (occurring between ~350 and 550 °C), although its space group (*Fmmm* [10], *Amam* [11, 12], or *B*2*cb* [13]) was under debate. Further experimental [14] and theoretical [15] investigations supported the existence of an intermediate paraelectric phase with *Amam* symmetry. Surprisingly, $SrBi_2Nb_2O_9$ shows a single crystallographic phase transition [16] from *A*21*am* to *I*4/*mmm*, rather than the proceeding via the intermediate phase, despite being isomorphous with SBT. Intermediate phases have not been detected in $Bi_4Ti_3O_{12}$ which seems to exhibit a direct phase transition from the high-temperature tetragonal to a ferroelectric phase. However, it was shown recently that the ferroelectric transition in BIT involves the interplay of six different normal modes belonging to four different irreducible representations, indicating that the apparent absence of intermediate phases remains to be explained [17].

The dynamics of the ferroelectric phase transition in SBT has been investigated by means of different spectroscopy techniques. Raman experiments associated the ferroelectric transition with the softening of a polar phonon mode. The lowest optical mode of 29 cm^{-1} at room temperature showed remarkable temperature variations towards T_c. Based on these findings it was suggested that the phase transitions in Bi-layered Aurivillius compounds are of displacive type [18]. A marked increase of damping near T_c indicated that the nature of the phase transition shows a crossing over from displacive to order–disorder type in the neighborhood of T_c [19, 20]. This dynamical behavior was also suggested from more recent Raman scattering investigations in SBT single crystals [21].

Surprisingly, terahertz (THz) spectroscopy studies showed that the soft mode with frequency near 29 cm^{-1} has shown no anomaly around T_c [22, 23]. Only a weak gradual softening of this mode was observed during heating up to 950 K and, consequently, its contribution to the low frequency permittivity is much smaller than that needed to account for the reported dielectric anomaly near T_c. An additional relaxation process below the phonon frequencies was resolved in the THz transmission spectra. The critical slowing down of its relaxation frequency would be responsible for the dielectric anomaly near the ferroelectric transition temperature. Therefore, it was proposed that the phase transition in SBT is prevailingly of order–disorder type [23]. It was also suggested the existence of polar clusters in the paraelectric phase, whose dynamics should be in origin of the critical relaxations [24].

Single crystal results are important to determine the anisotropy of material properties. However, the experimental studies of Aurivillius compounds are carried out mainly on ceramics and thin films and rarely on single crystals due to the lack of crystals of sufficiently good quality. As a consequence, the complete set of dielectric and piezoelectric coefficients of SBT has not been determined.

Given this controversial experimental background and the difficulties intrinsic to high-temperature measurements, finite-temperature simulations of Aurivillius compounds are highly desirable. In this paper we investigate the sequence and the local polarization dynamics of the transitions in SBT by using a shell-model approach with parameters fitted to first-principle calculations.

Shell-model approach and computational details

While first-principle calculations have contributed greatly to the understanding of the electronic structure and structural instabilities of SBT [6, 7, 25, 26] and related Aurivillius compounds [17, 27–29], these methods are restricted to studying zero-temperature properties. Nowadays, the combination of first-principle calculations with effective Hamiltonian [30, 31], or shell-model [32, 33] techniques offers a multiscale approach to investigate the various functional properties of ferroelectric oxides in terms of temperature, pressure, composition, and size. Both methods are able to correctly reproduce the phase sequences in many ABO_3 perovskites although the transition temperatures have relatively large errors.

In the shell-model approach, atomic interactions are represented by potentials between each pair of atoms in the system. Electronic polarization of the atoms is implemented via the Dick-Overhauser model [34], in which an atom is considered as a charged core connected to a massless charged shell. The equilibrium distance between the core and shell is a representation of the electronic polarization of that atom. The interactions between cores and shells are controlled by interatomic potentials whose parameters are fitted to achieve the best possible comparison with experiment or ab initio techniques.

The model used in this work contains fourth-order core–shell couplings (k_2, k_4), long-range Coulombic interactions and short-range interactions described by two different types of potentials. A Rydberg potential $V = (A + Br)\, e^{-r/\rho}$ is used for the Sr–O, Ta–O, and Bi–O pairs, and a Buckingham potential $V(r) = A\, e^{-r/\rho} + C/r^6$ is used for O–O interactions. For more details about the shell-model approach applied to ferroelectric materials see Ref. [33]. The model parameters were fitted completely to ab initio results. That is, no explicit experimental data had been used

as input. The local-density approximation (LDA) calculations were performed with the LAPW method, as implemented in the WIEN2k code [35]. Exchange and correlation effects were treated within the LDA using the parametrization by Perdew and Wang. The muffin-tin sphere radii $R_i = 2.0$, 1.8, 2.3, and 1.5 a.u. were used for Sr, Ta, Bi, and O, respectively. The value of the parameter RK_{max}, which controls the size of the basis set for the wave functions, was chosen to be 7.3 for all the calculations. This resulted in well-converged basis sets consisting of approximately 2500 LAPW functions. For the Sr-4*s* and 4*p*, Ta-5*s*, 5*p*, and 4*f*, Bi-6*s* and 5*d*, and O-2*s* states local orbitals were chosen in addition. Integrations in reciprocal space were performed using the tetrahedron method. We used a $6 \times 6 \times 6$ mesh which represents 28*k* points in the irreducible wedge for the body-centered tetragonal structure. Convergence tests indicate that only small changes result from going to a denser *k* mesh or to a larger value of RK_{max}. The input information for the fitting procedure corresponded to LDA results of the optimized crystal structure for the orthorhombic and tetragonal phases, energy as a function of volume and strain (*c*/*a*, *c*/*b*, *b*/*a*), underlying potential energy surfaces for structural distortions (ferroelectric and ferrodistortive) of the tetragonal phase, and forces between atoms. The shell-model parameters, shown in Table 1, were adjusted to the LAPW results using a least-square procedure.

The phase transition sequence and the dynamical properties of the material are investigated by molecular dynamics (MD) simulations using the DL-POLY package [36]. The runs were performed employing a Hoover constant-(σ, T) algorithm with external stress set to zero; all cell lengths and cell angles were allowed to fluctuate. Periodic boundary conditions over 7168 atoms were considered. The time step was 0.4 fs, which provided enough accuracy for the integration of the shell coordinates. The total time of each simulation, after 5 ps of thermalization, was 45 ps.

Table 1 Shell-model parameters for SBT

Atom	Core charge	Shell charge	k_2	k_4
Sr	−2.060	3.346	45.0	6464.8
Bi	8.575	−5.760	269.7	63.3
Ta	10.380	−5.492	1064.8	32.9
O	0.419	−2.274	17.2	1079.3
Short-range	A	B	ρ	C
Sr–O	872.043	−67.565	0.362147	0.0
Bi–O	24135.937	−9301.572	0.291147	0.0
Ta–O	4681.849	−689.125	0.290416	0.0
O–O	17585.281	0.0	0.239138	23.226

Units of energy, length, and charge are given in eV, Å, and electrons, respectively

Results and discussion

The resulting model is able to reproduce correctly the $T = 0$ K structure of SBT, and in good agreement with LDA. It gives an orthorhombic ground state (space group *A*21*am*) with lattice parameters $a = 5.46$ Å, $b = 5.44$ Å, and $c = 24.42$ Å, while the LDA results are $a = 5.49$ Å, $b = 5.48$ Å, and $c = 24.70$ Å. As it is well known, LDA underestimates volume and volume-dependent properties with respect to experimental values. For SBT the experimental lattice constants are $a = 5.52$ Å, $b = 5.52$ Å, and $c = 25.02$ Å [37]. So, the LDA underestimation of the static structural properties will be translated via the adjusted model to the finite-temperature behavior. Regarding the internal atomic positions, the relative coordinates of the orthorhombic *A*21*am* structure obtained by the model agree with experimental values better than 2% (see Table 2). The spontaneous polarization, however, is underestimated. The model gives a spontaneous polarization $P \approx 8$ μC/cm^2 along the *a*-axis. Although this value agree quite well with the polarization measured in SBT ceramics and thin films, it is lower than the value $P = 20$ μC/cm^2 measured in single crystals [38]. The absence of ferroelectricity along the [001] is in agreement with experiments [39, 40].

Table 2 Internal coordinates for the orthorhombic *A*21*am* structure obtained by the shell model (first line) compared with experimental data from Reference [36] (second line)

Atom	Position	*X*	*Y*	*Z*
Sr	4*a*	0	0.245	0
		0	0.256	0
Bi	8*b*	0.441	0.776	0.199
		0.463	0.776	0.199
Ta	8*b*	0.512	0.752	0.412
		0.510	0.748	0.414
O(1)	4*a*	0.515	0.292	0
		0.524	0.289	0
O(2)	8*b*	0.514	0.707	0.334
		0.521	0.699	0.341
O(3)	8*b*	0.717	0.998	0.251
		0.738	0.992	0.250
O(4)	8*b*	0.742	0.978	0.074
		0.755	0.986	0.070
O(5)	8*b*	0.791	0.972	0.585
		0.791	0.980	0.583

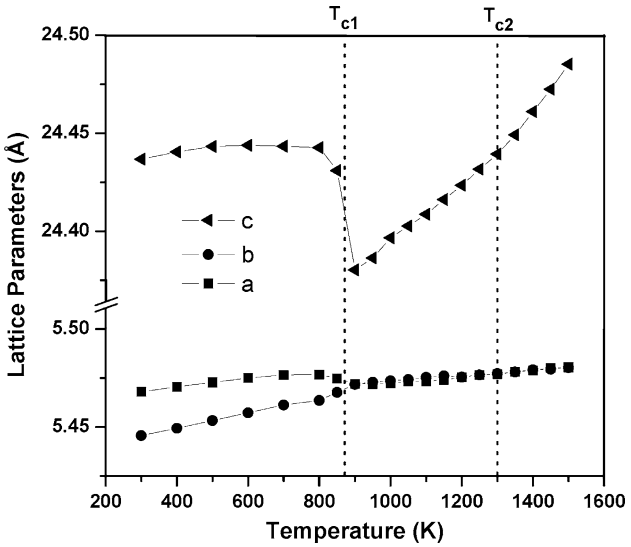

Fig. 1 Thermal evolution of lattice parameters for $SrBi_2Ta_2O_9$ determined from MD simulations. The *vertical lines* indicate the approximate positions of the structural phase transitions

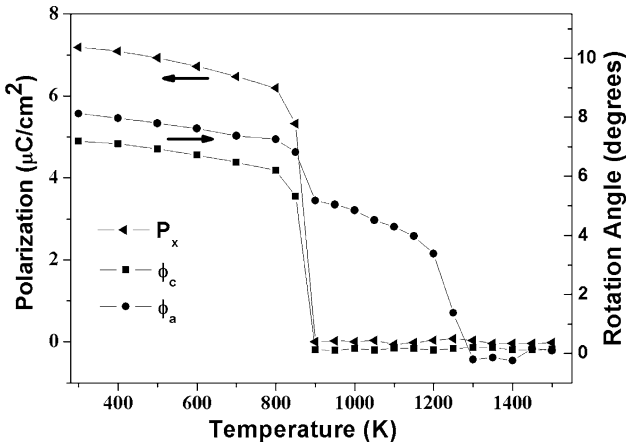

Fig. 2 Thermal evolution of the order parameters for $SrBi_2Ta_2O_9$ determined from MD simulations. P_x is the spontaneous polarization along the *a*-axis. Φ_a and Φ_c are the rotation angles of the TaO_6 octahedra around the *a* and *c* axes, respectively

The temperature-driven phase transition sequence given by the shell model is investigated from MD simulations. The lattice constants as a function of temperature are shown in the Fig. 1. Anomalies are clearly discernible in the plots of *a*, *b*, and *c* parameters versus *T*, suggesting the existence of two phase transitions, one at $T_{c1} \sim 870$ K and another at $T_{c2} \sim 1300$ K, the last one signed by a marked change of slope in the temperature behavior of the lattice parameters *c*. In fact, above 1300 K the lattice parameter *c* increases faster with temperature. To better characterize the transitions we define three order parameters which are related to the main distortions leading to the low-temperature phase from the tetragonal structure: (1) the spontaneous polarization (P_x) along the *a*-axis, (2) the rotation angles of the TaO_6 octahedra around the *a*-axis (Φ_a), and (3) the rotation angles of the octahedra around the *c*-axis (Φ_c). The behavior of the three order parameters as a function of temperature is shown in Fig. 2. At low temperatures ($T < T_{c1}$) the structure is orthorhombic ($a \neq b \neq c$) and P_x, Φ_a, and Φ_c are all clearly different from zero, indicating the presence of the *A*21*am* ferroelectric phase. The lattice parameters show strong anomalies at T_{c1}, despite the fact that the structure is still orthorhombic up to T_{c2}. In this temperature range ($T_{c1} < T < T_{c2}$) the lattice parameter *a* is slightly different from *b*; P_x and Φ_c are very close to zero while Φ_a remains finite. This indicates that a transition from the ferroelectric to an orthorhombic paraelectric phase takes place at T_{c1}. This transition involves not only loss of polarization, but also the loss of the TaO_6 octahedral tilt mode around the *c*-axis. The orthorhombic paraelectric structure is then characterized by the rotation of the TaO_6 octahedra around the *a*-axis. At T_{c2}, *a*, and *b* take the same value, and Φ_a vanishes. This is an indication that a transition to a tetragonal paraelectric *I4/mmm* phase occurs at this temperature. We conclude that the developed model reproduces correctly the non-trivial phase transition sequence of SBT.

Displacive and order–disorder characters can be distinguished by inspecting the distribution of the local polarization vectors in the paraelectric phase just above the transition. A displacive (locally non-polar) or order–disorder (locally polar) transition should be characterized by a single-peaked and a double-peaked structure, respectively. The distribution of the *x* component of the local polarization at 500, 900, 1000, and 1400 K is shown in Fig. 3. The local polarization has been defined as the polarization of a single primitive cell of the *A*21*am* orthorhombic structure, containing two $SrBi_2Ta_2O_9$ molecules per cell. At 500 K

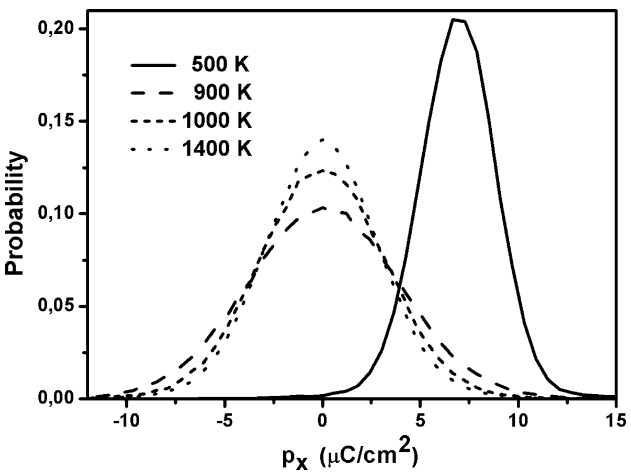

Fig. 3 The probability distribution of the Cartesian component of the local polarization p_x at different temperatures

the system is in the orthorhombic ferroelectric phase and the distribution presents a single peak centered at the average polarization of the system at that temperature ($\approx$7 μC/cm^2). In both paraelectric phases, intermediate orthorhombic (1000 K) and high-temperature tetragonal (1400 K), the distributions show a single peak structure. This structure remains unchanged even very close to the Curie temperature T_{c1} (see the plot for 900 K), which indicates a predominant displacive character for the ferroelectric transition.

The time evolution of local polarization components is shown in Fig. 4. At 500 K, the cartesian component p_x shows fast oscillations around a finite polarization value, and y and z components are oscillating around zero, in concordance with the macroscopic spontaneous polarization which is developed along the a direction. Just above the transition at 900 K, the x component shows fast oscillations around zero. This behavior persists in tetragonal paraelectric phase at 1400 K. In order–disorder ferroelectric perovskites, such as $KNbO_3$ or $BaTiO_3$, the local polarization dynamics in the paraelectric phase is characterized by the presence of fast oscillations around finite polarization values which coexist with much slower polarization reversals. So, the order–disorder dynamics possess two components with different time scales, while one component is associated with quasi-harmonic oscillations around an off-center position, the other refers to a relaxational motion between equilibrium sites. Clearly this is not the case observed here, where a fast oscillatory dynamics around zero polarization indicates a displacive-like dynamics for the local polarization near the ferroelectric transition. This supports the idea that the additional relaxation process observed in the THz transmission spectra could be of extrinsic nature, as it was originally suggested [22].

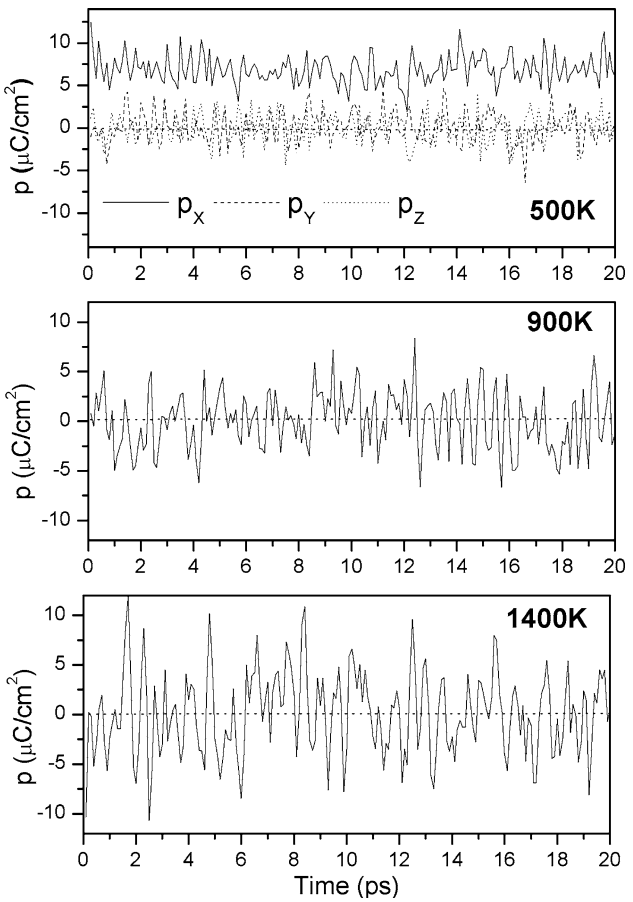

Fig. 4 Time evolution of a cell polarization at different temperatures. At 900 and 1400 K only the x component is shown

One advantage of our approach is the possibility to calculate single crystal properties. Single crystal results are important to determine the anisotropy of material properties. We used the atomistic model to investigate the dielectric and piezoelectric properties of SBT through the calculation of the dielectric constants (ε) and piezoelectric coefficients (d) along crystallographic directions. In order to calculate them, we compute at each temperature the changes produced by applied electric fields in the polarization and in strains components, respectively. Figure 5 shows the dielectric susceptibilities along crystallographic directions ε_{11}, ε_{22}, and ε_{33} as a function of temperature. We choose the polar direction along the z-axis, in such a way that the a, b, and c axes of the orthorhombic phase correspond to the 3, 1, and 2 directions, respectively. The behavior showed in Fig. 5 is in qualitative agreement with experimental measurements in single crystals [38], although in the latter the in-plane anisotropy (ε_{11} and ε_{33}) was not distinguished. The maximum of ε_{33} corresponds to the ferro–paraelectric phase transition observed at T_{c1}. No

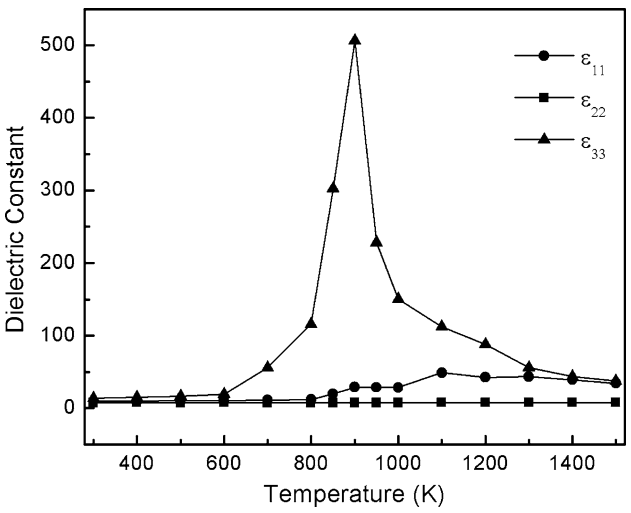

Fig. 5 Temperature dependence of the dielectric permittivity along the crystallographic directions for SBT determined from MD simulations

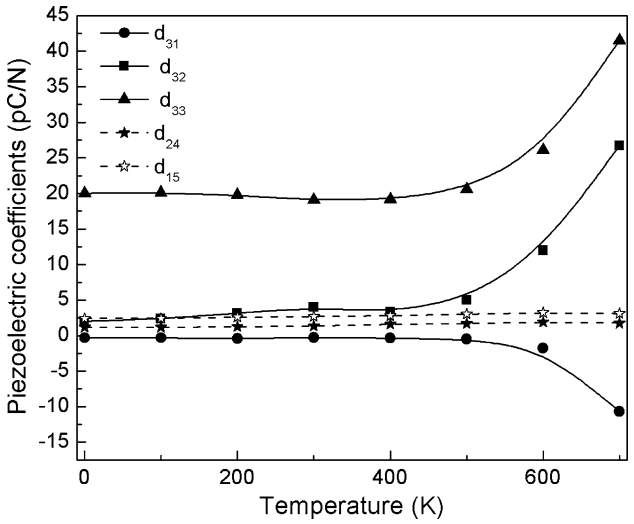

Fig. 6 Piezoelectric coefficients as a function of temperature in SBT obtained through MD simulations

anomalies are observed in ε_{11} and ε_{22} at this temperature, which confirms that the small peak observed experimentally along the orthorhombic c-axis (ε_{22} here) around T_{c1} [38] is of extrinsic character. No dielectric anomalies are observed at the paraelectric–paraelectric phase transition T_{c2}. However, the anisotropy of the system in the intermediate phase can be distinguished through the dielectric behavior. While in the tetragonal phase ($T > T_{c2}$) a and b axes are equivalent and $\varepsilon_{11} = \varepsilon_{33}$, ε_{33} is considerable larger than ε_{11} in the intermediate phase ($T_{c1} < T < T_{c2}$). That difference arises from the atomic displacements along the b direction produced by the rotation of TaO_6 octahedra around the a-axis. The anisotropy of the dielectric response in the a–b plane provides an alternative way for the identification of the intermediate phase, and it can be used for the experimental detection of intermediate phases in other Aurivillius compounds, provided the existence of single crystals of sufficient quality.

The thermal evolution of the piezoelectric constants obtained from the simulations is shown in Fig. 6. From symmetry considerations, there are five independent piezoelectric coefficients for the ferroelectric orthorhombic phase of SBT: the longitudinal d_{33}, the transverse d_{31} and d_{32}, and the shear components d_{15} and d_{24} [41]. We observe that the coefficients are rather small and they increase near the ferroelectric transition temperature T_{c1}. At room temperature the theoretical value of d_{33} is $\sim$20 pC/N, while the reported experimental values for ceramic samples are between 12 pC/N and 20 pC/N [42, 43]. Regarding the transverse coefficients, the values obtained from the simulation are $d_{32} = 4$ pC/N and $d_{31} = -0.5$ pC/N. One interesting characteristic of SBT is the relatively large hydrostatic charge coefficient $d_h = d_{33} + d_{32} + d_{31}$, which is comparable to that of conventional PZT ceramics [40]. Such particular behavior is mainly due to the effective positive contribution of the transverse coefficients $d_{32} + d_{31}$, which is correctly described by our atomistic model. While it is not possible to distinguish between both coefficients in ceramics, our single crystal calculations show that the contribution comes from the positive value of d_{32} (the strain along c-axis).

Conclusions

We have shown that the combination of first-principle calculations with shell-model techniques offers a multiscale approach to investigate finite-temperature properties of Aurivillius compounds. In particular, we demonstrated the existence of an intermediate paraelectric phase in SBT without using any explicit experimental data as input; this phase naturally emerges from the simulated phase diagram. The local polarization dynamics near the ferroelectric transition does not provide any indication of a relaxation process. Finally, the dielectric and piezoelectric coefficients along crystallographic directions were evaluated.

Acknowledgements We thank R. Migoni for useful discussions. This work was sponsored by Consejo Nacional de Investigaciones Científicas y Tecnológicas de la Republica Argentina (CONICET). MGS thanks support from CIUNR.

References

1. Scott JF (2000) Ferroelectric memories. Springer-Verlag, Berlin Heidelberg
2. Kholkin AL, Brooks KG, Setter N (1997) Appl Phys Lett 71:2044
3. Aurivillius B (1949) Ark Kemi 1:463
4. Smolenskii GA, Isupov VA, Agranovskaya AI (1961) Sov Phys Solid State 3:51
5. Rae AD, Thompson JG, Withers RL (1992) Acta Cryst B 48:418
6. Stachiotti MG, Rodriguez CO, Ambrosch-Draxl C, Christensen NE (2000) Phys Rev B 61:14434
7. Perez-Mato JM, Aroyo M, Garcia A, Blaha P, Schwarz K, Schweifer J, Parlinski K (2004) Phys Rev B 70:214111
8. Newnham RE, Wolfe RW, Dorrian JF (1971) Mater Res Bull 6:1029
9. Reaney IM, Roulin M, Schulman HS, Setter N (1995) Ferroelectrics 165:295
10. Onodera A, Kubo T, Yoshio K, Kojima S, Yamashita H (2000) Jpn J Appl Phys 39:5711
11. Hervoches CH, Irvine JTS, Lightfoot P (2001) Phys Rev B 64:100102
12. Macquart R, Kennedy BJ, Brett AH, Howard CJ, Shimakawa Y (2002) Integr Ferroelectr 44:101
13. Kim JS, Cheon C, Shim H-S, Lee CL (2001) J Eur Ceram Soc 21:1295
14. Kamba S, Pokorny J, Porokhonskyy V, Petzelt J, Moret MP, Garg A, Barber ZH, Zallen R (2002) Appl Phys Lett 81:1056
15. Machado R, Sepliarsky M, Stachiotti MG (2008) Appl Phys Lett 93:242901

16. Snedden A, Hervoches CH, Lightfoot P (2003) Phys Rev B 67:92102
17. Perez-Mato JM, Blaha P, Schwarz K, Aroyo M, Orobengoa D, Etxebarria I, García A (2008) Phys Rev B 77:184104
18. Liu J, Zou G, Yang H, Cui Q (1994) Solid State Commun 90:365
19. Kojima S (1998) J Phys Condens Matter 10:327
20. Kojima S, Saitoh I, Yamamoto T (1998) In: Proceedings of the eleventh IEEE international symposium on applications of ferroelectrics, p 471
21. Almeida A, Chaves MR, Amorin H, Costa MEV, Kholkin AL (2005) J Phys Condens Matter 17:7605
22. Kempa M, Kuzel P, Kamba S, Samoukhina P, Petzelt J, Garg A, Barber ZH (2003) J Phys Condens Matter 15:8095
23. Kadlec F, Kamba S, Kuzel P, Kadlec C, Kroupa J, Petzelt J (2004) J Phys Condens Matter 16:6763
24. Nuzhnyy D, Kamba S, Kužel P, Veljko S, Bovtun V, Savinov M, Petzelt J, Amorín H, Costa MEV, Kholkin AL, Boullay P, Adamczyk M (2006) Phys Rev B 74:134105
25. Miura K (2002) Appl Phys Lett 80:2967
26. Zhang J, Yin Z, Zhang MS (2002) Appl Phys Lett 81:4778
27. Machado R, Stachiotti MG, Migoni RL, Tera AH (2004) Phys Rev B 70:214112
28. Hashimoto T, Moriwake H (2008) Phys Rev B 78:092106
29. Xu B, Yi L (2007) J Alloys Compd 438:25
30. Vanderbilt D (1997) Curr Opin Solid State Mater Sci 2:701
31. Ponomareva I, Naumov I, Kornev I, Fu H, Bellaiche L (2005) Curr Opin Solid State Mater Sci 9:114
32. Sepliarsky M, Asthagiri A, Phillpot SR, Stachiotti MG, Migoni RL (2005) Curr Opin Solid State Mater Sci 9:107
33. Sepliarsky M, Stachiott MG, Phillpot SR (2005) In: Yip S (ed) Handbook of materials modeling. Springer, New York
34. Dick BG, Overhauser AW (1958) Phys Rev 112:603
35. Blaha P, Schwarz K, Madsen GKH, Kvasnicka D, Luitz J, WIEN2K (2001) An augmented plane wave + local orbitals program for calculating crystal properties. Karlheinz Schwarz, Techn. Universität Wien, Austria
36. DL-POLY is a package of molecular simulation routines written by W. Smith and T. R. Forester, Daresbury and Rutherford Appleton Laboratory, Daresbury, UK
37. Shimakawa Y, Kubo Y, Nakagawa Y, Goto S, Kamiyama T, Asano H, Izumi F (2000) Phys Rev B 61:6559
38. Amorin H, Shvartsman VV, Kholkin AL, Costa MEV (2004) Appl Phys Lett 85:5667
39. Desu SB, Vijay DP, He B (1996) Appl Phys Lett 69:1719
40. Garg A, Barber ZH, Dawber M, Scott JF, Snedden A, Lighfoot P (2003) Appl Phys Lett 83:2414
41. Nye JF (2000) Physical properties of crystals. Clarendon Press, Oxford
42. Jain R, Chauhan AKS, Gupta V, Sreenivas J (2005) J Appl Phys 97:124101
43. Sun L, Feng C, Chen L, Huang S, Wen X (2006) Mater Sci Eng B 135:60